

Suppression of rotating external kink instabilities using optimized mode control feedback

Alexander J. Klein, David A. Maurer, Thomas Sunn Pedersen, Michael E. Mael, Gerald A. Navratil, Cory Cates, Mikhail Shilov, Yuhong Liu, Nikolai Stillits, and Jim Bialek
Plasma Physics Laboratory, Columbia University, New York, New York 10027

(Received 14 December 2004; accepted 18 January 2005; published online 24 March 2005)

Rotating external kink instabilities have been suppressed as well as excited in a tokamak using active magnetic coils that directly couple to the plasma through gaps in passive stabilizing conducting shells that surround the plasma. The kink instability has a complex growth rate, approximately $(3+i2\pi5)\times 10^3\text{ s}^{-1}$, and is near the ideal wall stability limit when discharges are prepared with a rapid plasma current ramp and adjusted to have an edge safety factor near 3. The active control coils are driven by a digital mode control feedback system that uses multiple field-programmable gate arrays to analyze signals from 20 poloidal field sensors and achieve high-speed feedback control. The feedback coil geometry used was designed to optimize feedback effectiveness. Signal processing is of critical importance to optimize phase transfer functions for control of rotating modes. © 2005 American Institute of Physics. [DOI: 10.1063/1.1868732]

External kink instabilities in tokamaks are driven by radial gradients of the plasma current,¹ and they set the stability limit of high beta tokamak plasmas.² The stability of the external kink depends significantly on the location and conductivity of a wall surrounding the plasma. For a perfectly conducting wall, the stability limit increases because eddy currents in the wall generate fields to oppose the helical kink perturbation. For any wall configuration, the ideal wall stability limit can be calculated using a three-dimensional (3D) electromagnetic code, like VALEN,³ and an ideal magnetohydrodynamic (MHD) stability code, like DCON.⁴ For a wall with finite conductivity, the wall eddy currents decay, and the external kink instability is called the resistive wall mode (RWM) when the plasma is above the no-wall stability limit but below the ideal wall stability limit.⁵ Although the RWM grows slowly at a rate proportional to the eddy current decay rate γ_w , the RWM instability must be prevented in order to operate steady-state tokamak reactors with both high bootstrap current fraction and high fusion power density.^{6,7}

Previous experiments have demonstrated stabilization of the external kink with a conducting wall⁸ and stabilization of the RWM instability either by plasma rotation^{9,10} or by active feedback control.^{11,12} In rotating plasma, plasma dissipation stabilizes the RWM^{13,14} when the rate of dissipation exceeds the rate at which energy is released from a slowly growing (in proportion to γ_w) kink perturbation. Although the physics of RWM stabilization due to rotation remains a subject of study, recent measurements using the HBT-EP tokamak¹⁵ have shown rotationally stabilized kink perturbations to be consistent with a semiempirical viscous model of Fitzpatrick¹⁶ in the high-dissipation regime. Near the ideal wall stability limit, the RWM is stable when the plasma rotation Ω exceeds a critical value dependent upon the dissipation rate ν_d ,

$$\Omega_{crit} = 2\gamma_{MHD}\sqrt{\gamma_w/\nu_d}, \quad (1)$$

where γ_{MHD} is the ideal MHD growth rate of the external kink at the no-wall limit. The external kink growth rate for rotating plasma at the ideal wall limit is $\gamma \approx i\Omega + (\gamma_{MHD}^2/\nu_d) \times (S-1)$, where S is a normalized stability parameter. Kink instability results when S exceeds the ideal wall limit or when $S > 1$. S can be calculated with an ideal MHD code, it is defined as the ratio of the ideal kink perturbed energy δW calculated without a wall, to the difference of the perturbed vacuum energy when evaluated with and without an ideal wall. High plasma dissipation slows the kink mode growth rate from its usual value¹⁷ by the factor $\nu_d/\gamma_{MHD} > 1$.

While feedback control of the slow RWM has been demonstrated, feedback control near the ideal wall limit requires consideration of both the marginally stable external kink that rotates with the plasma Ω and the RWM that rotates much more slowly at a rate near $\gamma_w \ll \Omega$.¹⁶ Near the ideal wall stability limit in rotating plasma, the dominant frequency of interest will be $|\gamma| \sim \Omega$, and the active feedback controller must be capable of high-speed control with low latency. In addition, limitations to the feedback system arise from (1) the mutual inductive coupling between control and sensor coils (leading to self-oscillations and ceilings on attainable gain, as well as noise), (2) coupling between the control coils and the conducting shell (leading to finite response time of the system, as well as limiting the stability range over which fixed feedback coefficients are effective¹⁸), and (3) coupling between the sensor coils and conducting shells that slow the response time of the feedback control fields. When these limitations are eliminated, we describe feedback as “optimized mode control.” Numerical modeling has predicted external kinks can then be feedback controlled up to the ideal wall limit.³

In this paper, we report the first successful use of optimized mode control of rotating external kink instabilities at the ideal wall limit. External kink instabilities are excited in

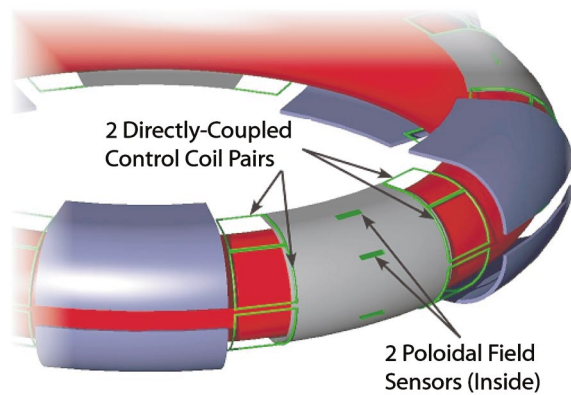


FIG. 1. (Color). Experimental arrangement of conducting shells, mode control coils, and poloidal field sensors.

the HBT-EP tokamak using a rapid plasma current ramp that creates growing helical perturbations with poloidal and toroidal mode numbers resonant with the edge safety factor, $m/n \sim q_a$. The feedback control coils directly couple to the plasma surface through toroidal gaps in the conducting shells, and the sensor coils were located to eliminate coupling to the control coils. Additionally, high-speed digital processing is used to measure and isolate the $n=1$ toroidal mode in real time so that each sensor provides only part of a larger signal array, reducing noise. The resulting configuration constitutes a highly optimized way to perform feedback control of external kink modes in toroidal plasmas.

The experiments were performed on the HBT-EP, a tokamak specifically designed for investigation of the effects of conducting walls and active feedback control configurations on MHD instabilities.^{8,11,15} The experimental arrangement is depicted in Fig. 1. Moveable wall segments at ten toroidal positions on the outboard side surround the plasma torus. Half of the segments are made from 1.2 cm thick aluminum (Al), at five toroidal positions, while half are made from 0.2 cm stainless steel (SS) which are interspersed between the Al shells (see Fig. 1). Adjusting the positions of the wall segments allows adjustment of the plasma-wall coupling (and the ideal wall stability limit) and wall current decay rate γ_w . When the Al segments are moved from the fully withdrawn to fully inserted position, the ideal wall limit doubles, and γ_w decreases from 6.3 to 2.3 ms⁻¹ for $m/n = 3/1$ modes.

The feedback control coils are mounted in the gaps between the aluminum and steel shells (Fig. 1) so that applied radial fields can couple directly to the plasma. A total of 40 control coils are arranged at four poloidal locations and at ten, equally spaced, toroidal positions. Each pair of control coils mounted on the same segment and at the same poloidal position is connected in series. Twenty sensors are also mounted onto the SS segments and positioned on the plasma facing side, so as to measure kink perturbations even for time-scales short compared with the SS wall's magnetic diffusion time. The mutual inductance between the poloidal sensors and the feedback coils has been measured to be negligible. There are four poloidal sensors at each of the five toroidal locations, forming an array of 20 sensors.

This configuration is significantly different from the so-called “smart-shell” control coils used previously.¹¹ Since the sensor and control coils have little or no mutual inductance, the feedback system is largely immune to self-oscillations that limited the previous feedback system at high gain. Solid-state 200 W audio amplifiers drive each control coil pair. We measured the maximum achievable gain in the absence of a plasma, using an external magnetic field pulse as an initial perturbation, to be ≈ 40 times greater than that used in the experiments. As the gain limits in the experiments are set by the available control power, the 40 times gain should be achievable with installation of higher power control coil amplifiers.

Calculations with the VALEN code³ were used to estimate the effectiveness of active feedback control of nonrotating external kink modes using the actual HBT-EP coil, wall, and sensor geometry. In the calculations, the gain was defined as the ratio of the voltage applied to the control coils to the perturbed poloidal flux measured by the sensor. When the gain was increased to 1×10^7 V/Weber, VALEN predicts kink stabilization at the ideal wall limit for HBT-EP. The measured gain in the experiment is 1.4×10^7 V/Weber.

Mode control feedback is achieved by detection of the $n=1$ toroidal component of the perturbed poloidal field and applying, in proportion, a toroidally rotated $n=1$ radial field with the control coils. The sensors signals are amplified and filtered using analog circuitry, and then digitized to 16 bits for input to multiple, high speed field-programmable gate arrays (FPGA).¹⁹ Data are sampled with a sample interval, $\tau_s = 10 \mu\text{s}$. After temporal filtering (described in the next paragraph), five sensor signals at each of four poloidal positions (and at equally spaced toroidal angles) are digitally processed to select the $n=1$ component of the measured magnetic field perturbation. The $n=1$ component is isolated using a discrete Fourier transform (DFT), and the $n=0$ and $n=2$ components are disregarded. Each poloidal group is processed independently from the others, and the toroidal phase at each poloidal angle is determined by appearance of the $n=1$ mode at each poloidal location.

A rotation operator is used to generate the appropriate toroidal phasing of the radial control fields, and an inverse DFT produces control outputs that are sent to the audio amplifiers. Except for the temporal filter, the entire digital algorithm is implemented as a 5×5 matrix multiplication,

$$\vec{V}_c = G \times (\overrightarrow{DFT}^T \cdot \vec{R} \cdot \vec{N}_1 \cdot \overrightarrow{DFT}) \cdot \vec{\delta\Phi}_s = G \times \vec{A} \cdot \vec{\delta\Phi}_s, \quad (2)$$

where V_c is the control coil voltage, $\delta\Phi_s$ is the poloidal field sensor flux, N_1 represents $n=1$ mode isolation, R is a toroidal rotation, and G is the effective overall system gain. Since the FPGAs function in parallel, the matrix processing in Eq. (1) can be accomplished in less than 0.1 μs ; however, the system latency is limited by the analog to digital conversion times to be approximately 10 μs .

A second-order digital filter is used to adjust the overall frequency-dependent gain and phase of the feedback system [i.e., the complex gain inherent in G in the Laplace transform of Eq. (1)]. We find the effectiveness and stable phase margin of the feedback system depends strongly on the particular

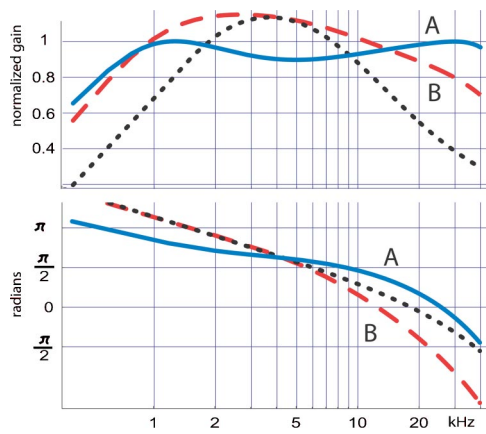


FIG. 2. Normalized overall feedback gain G illustrating the frequency variation of the magnitude and phase. Shown are: dotted line intrinsic to analog hardware, dashed line with the effect of filter B , solid line with the effect of filter A .

digital filter applied prior to the mode decomposition. Two different digital filters were used for two sets of experiments. These filters are second-order phase lead/lag compensating algorithms, hence forth referred to as filters A and B . For filter A , the phase variation was kept as small as possible. For filter B , the phase of the overall gain varied strongly throughout the band of interest, $1 \text{ kHz} < f < 20 \text{ kHz}$, which is similar to the type of phase transfer that results when the system latency is increased. The compensator that provided the flattest frequency response (A) resulted in the best performance of the feedback system, as will be discussed in Sec. IV. The normalized overall transfer functions of the feedback system are shown in Fig. 2.

Rotating external kink instabilities appear in HBT-EP discharges when the plasma current increases rapidly, $\sim 2 \text{ MA/s}$, and when the edge safety factor q_a decreases below 3. This discharge programming broadens the current profile, increases the external kink drive, and reduces the growth of internal tearing modes. For the discharges described here (Fig. 3), q_a remained near 3 for more than 1 ms, and rotating $m/n=3/1$ kink modes grew on a time scale of $\sim 0.3 \text{ ms}$. A

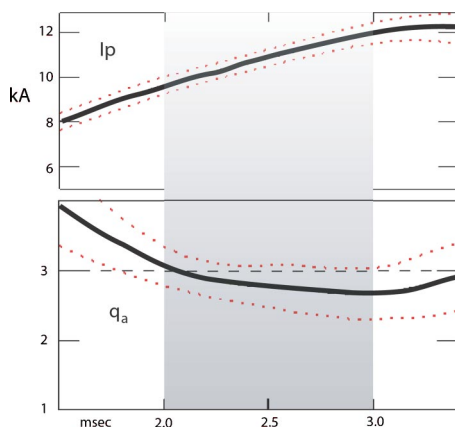


FIG. 3. Shot-averaged evolution of the plasma current and edge safety factor. Investigation of feedback effectiveness was performed during the time interval between $2 \text{ ms} < t < 3 \text{ ms}$, when rotating external kink instabilities appeared.

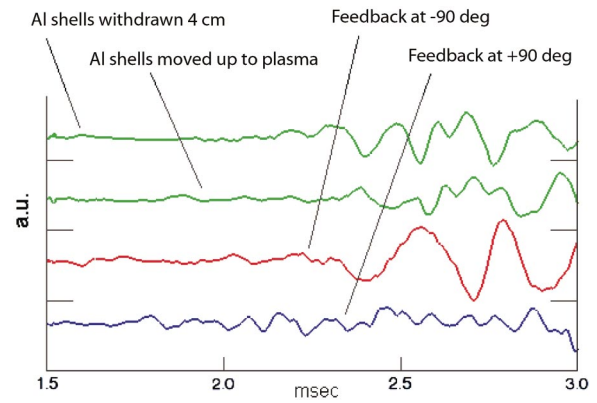


FIG. 4. (Color). Poloidal field measurements of $m=3$ Rogowski oscillations for four cases: no feedback Al wall retracted by 4 cm, no feedback with Al wall fully inserted, positive feedback (amplification), and negative feedback.

variety of magnetic diagnostics identified the mode's helical $3/1$ structure. The kink mode rotated toroidally, in a manner similar to previous observations for the $m/n=2/1$ tearing mode:²⁰ in the electron diamagnetic drift direction and at a frequency near 5 kHz. In the absence of any feedback, the kink mode growth rate is approximately $(3+i2\pi 5) \times 10^{-3} \text{ s}^{-1}$. For these discharges, $\gamma_{\text{MHD}} \sim 50-100 \times 10^{-3} \text{ s}^{-1}$ and $5 < v_d / \gamma_{\text{MHD}} < 8$ for HBT-EP.¹⁵ The measured kink growth rate is consistent with expectations near the ideal wall limit, $S \sim 1$. These parameters predict RWM stabilization for plasma rotation exceeding a critical value, $\Omega/2\pi > 3 \text{ kHz}$. The growth rate of the kink instability was observed to be independent of the position of the Al wall segments as expected for rotating kink instabilities at the ideal wall limit. As the Al wall segments were fully inserted, the characteristics of the kink instability did not change as illustrated in Fig. 4.

When active feedback was applied, the closed-loop kink mode response depended strongly on the toroidal rotation, or phase, represented by the matrix R in Eq. (1). The helical geometry of the $n=1$ external kink mode has a maximum of the perturbed poloidal field located at a 90° toroidal angle from the maximum perturbed radial fields at the plasma surface. Maximum feedback suppression (or “negative” feedback) occurs when the toroidal phase between the applied and the sensed signals is 90° . When the toroidal phase rotation is programmed to be opposite (i.e., -90°), then maximum mode excitation results, corresponding to “positive” feedback. Figure 4 also shows examples of the detected $m/n=3/1$ oscillations resulting from feedback that tracked the rotating kink instability with toroidal phase of $\pm 90^\circ$ relative to the $n=1$ phase of the sensor signals.

The toroidal phase rotation operator for each of the four poloidal groups of sensor/control coils was adjusted for 144 similar discharges in 5 deg increments. 72 discharges were run using A digital filter, and 72 using B digital filter. The resonant $m/n=3/1$ signals from a Fourier analyzing, $m=3$, Rogowski coil was used to detect the closed-loop plasma response. The temporal Fourier transform of the Rogowski coil signal was computed in the time interval $2 \text{ ms} < t < 3 \text{ ms}$ for each discharge, and the amplitude of the resonant

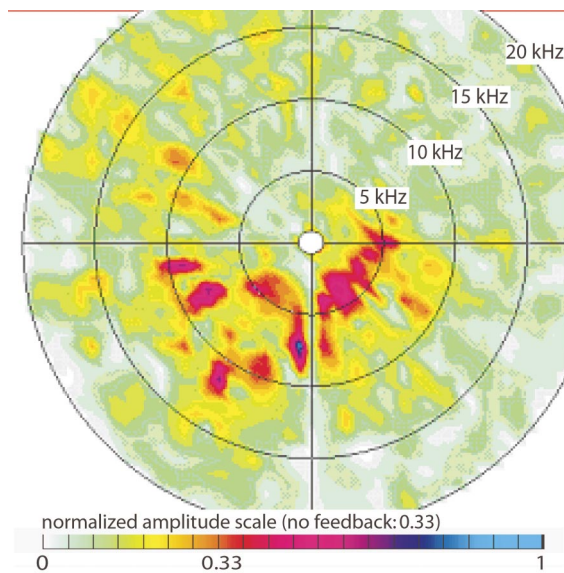


FIG. 5. (Color). Amplitude of the frequency spectrum of $m=3$ Rogowski coil oscillations as a function of the feedback toroidal rotation angle R for filter A. Angle represents phase difference between applied radial magnetic field component and sensed poloidal component. The large phase margin is obtained with effective phase compensation.

poloidal field fluctuations were displayed in polar density plots for the frequency band from $1 \text{ kHz} < f < 20 \text{ kHz}$. Figure 5 summarizes the resonant kink response for filter A and Fig. 6 summarizes the results for filter B. In each plot, the distance from the origin is proportional to frequency, and the polar angle represents the toroidal target phase between control and sensor fields, i.e., the toroidal angle between the applied radial magnetic field and measured perturbed poloidal field.

The polar response plots directly display the closed-loop phase-margins obtained with each filter. As is clearly evident,

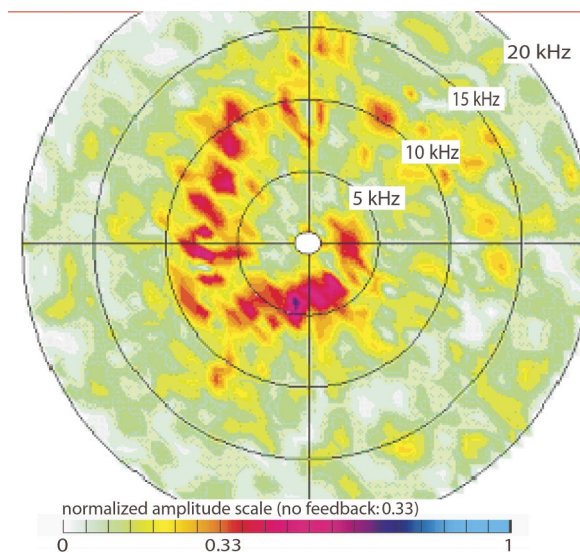


FIG. 6. (Color). Amplitude of the frequency spectrum of $m=3$ Rogowski coil oscillations for filter B. Angle represents phase difference between applied radial magnetic field component and sensed poloidal component. Because of the appearance of oscillations at $\sim 10 \text{ kHz}$, the phase margin nearly vanishes with ineffective phase compensation.

the filter B results in kink mode suppression within a narrow range of rotation angles at the natural mode frequency. However, closed-loop feedback with this filter also excites higher frequency oscillations near 10 kHz. At nearly all toroidal rotation angles, some level of $m=3$ oscillations are observed within some frequency band. The spiral pattern in Fig. 5 shows a frequency “pulling” to higher frequencies when the control coil phase lags the detected mode and a slight reduction in frequency when the control coils lead the detected kink modes. Figure 5 shows the plasma response for filter A corresponding to a nearly flat phase response. With this filter, kink modes can be completely suppressed within a rotational phase margin of $\approx \pm 45^\circ$ from the phase, 90° that provides negative feedback. With the opposite phase, the feedback control is set to reinforce the plasma fields, and kink excitation is observed.

In summary, optimized mode control experiments have suppressed, and excited, the $m/n=3/1$ rotating external kink mode. The instabilities are excited with a strong plasma current ramp and appear with parameters corresponding to the ideal wall stability limit. The active feedback coils are optimized since (1) the control coils couple directly to the plasma, (2) sensors couple directly to the plasma, and (3) controls and sensors have little or no mutual inductance. A high-speed digital controller using multiple FPGAs allow isolation of the $n=1$ component of the poloidal field perturbations and produce low-noise mode control with a system latency is less than the characteristic growth time of the mode.

The authors gratefully acknowledge the technical support of N. Rivera, J. Andreello, and J. Moran during the course of this work.

This work was supported by the U.S. Department of Energy Grant No. DE-FG02-86ER53222.

¹V. D. Shafranov, *Sov. Phys. Tech. Phys.* **15**, 175 (1970).

²E. J. Strait, *Phys. Plasmas* **1**, 1415 (1994).

³J. Bialek, A. H. Boozer, M. E. Mauel, and G. A. Navratil, *Phys. Plasmas* **8**, 2170 (2001).

⁴A. H. Glasser and M. S. Chance, *Bull. Am. Phys. Soc.* **42**, 1848 (1997).

⁵D. Pfirsch and H. Tasso, *Nucl. Fusion* **11**, 259 (1971).

⁶K. J. Manickam, G. Rewoldt, and T. M. Tang, *Phys. Rev. Lett.* **72**, 1212 (1994).

⁷A. Turnbull, T. S. Taylor, Y. R. Lin-Liu, and H. St. John, *Phys. Rev. Lett.* **74**, 718 (1995).

⁸T. H. Ivers, E. Eisner, A. Garofalo *et al.*, *Phys. Plasmas* **3**, 1926 (1996).

⁹A. M. Garofalo, A. D. Turnbull, E. J. Strait *et al.*, *Phys. Plasmas* **6**, 1893 (1999).

¹⁰A. M. Garofalo, E. J. Strait, L. C. Johnson *et al.*, *Phys. Rev. Lett.* **89**, 235001 (2002).

¹¹C. Cates, M. Shilov, M. E. Mauel, G. A. Navratil, D. Maurer, S. Mukherjee, D. Nadle, J. Bialek, and A. H. Boozer, *Phys. Plasmas* **7**, 3133 (2000).

¹²A. M. Garofalo, E. J. Strait, J. Bialek *et al.*, *Nucl. Fusion* **40**, 1491 (2000).

¹³A. Bondeson and D. J. Ward, *Phys. Rev. Lett.* **72**, 2709 (1994).

¹⁴M. S. Chu, J. M. Greene, T. H. Jensen, R. L. Miller, A. Bondeson, R. W. Johnson, and M. E. Mauel, *Phys. Plasmas* **2**, 2236 (1995).

¹⁵M. Shilov, C. Cates, R. James *et al.*, *Phys. Plasmas* **11**, 2573 (2004).

¹⁶R. Fitzpatrick, *Phys. Plasmas* **9**, 3459 (2002).

¹⁷L. E. Zakharov and S. V. Putvinskii, *Sov. J. Plasma Phys.* **13**, 118 (1987).

¹⁸A. H. Boozer, *Phys. Plasmas* **11**, 110 (2004).

¹⁹National Instruments: “7831-R” modules with Xilinx II processors.

²⁰E. Taylor, C. Cates, M. E. Mauel, D. A. Maurer, D. Nadle, G. A. Navratil, and M. Shilov, *Phys. Plasmas* **9**, 3938 (2002).